

Pre-landslide topographic reconstruction in Baetis Chaos, mars using a CaSSIS Digital Elevation Model

A. Guimpier, S. J. Conway, M. Pajola, A. Lucchetti, E. Simioni, C. Re, A. Noblet, N. Mangold, N. Thomas, G. Cremonese

▶ **To cite this version:**

A. Guimpier, S. J. Conway, M. Pajola, A. Lucchetti, E. Simioni, et al.. Pre-landslide topographic reconstruction in Baetis Chaos, mars using a CaSSIS Digital Elevation Model. Planetary and Space Science, 2022, 218, 10.1016/j.pss.2022.105505 . insu-03682332

HAL Id: insu-03682332
https://insu.hal.science/insu-03682332

Submitted on 14 Oct 2022

HAL is a multi-disciplinary open access archive for the deposit and dissemination of scientific research documents, whether they are published or not. The documents may come from teaching and research institutions in France or abroad, or from public or private research centers.

L'archive ouverte pluridisciplinaire **HAL**, est destinée au dépôt et à la diffusion de documents scientifiques de niveau recherche, publiés ou non, émanant des établissements d'enseignement et de recherche français ou étrangers, des laboratoires publics ou privés.

Pre-landslide topographic reconstruction in Baetis Chaos, Mars using a CaSSIS Digital Elevation Model.

A. Guimpier[1]*, S. J. Conway[1], M. Pajola[2], A. Lucchetti[2], E. Simioni[2], C. Re[2], A. Noblet[1], N. Mangold[1], N. Thomas[3], G. Cremonese[2] and CaSSIS Team.

[1]Laboratoire de Planétologie et Géosciences, UMR6112 CNRS, Nantes Université, Université d'Angers, Le Mans Université, France

[2]INAF - Astronomical Observatory of Padova, Italy

[3]University of Bern, Switzerland

**corresponding author* anthony.guimpier@univ-nantes.fr

Abstract

Planview detailed morphological analysis of martian landslides is usually performed using orbital imagery such as from the ConTeX camera (CTX) at 6 m/pix, the Colour and Stereo Surface Imaging System (CaSSIS) at 4.5 m/pix or the High-Resolution Imaging Science Experiment (HiRISE) at 0.25-0.5 m/pix. However, topographic information is key to fully understand a landslide's formation mechanism and its mobility, by estimating the material volumes mobilised and the spatial distribution of erosion and deposition. Digital Elevation Models (DEM) are required to carry out these analyses; nevertheless, there is a currently gap in landslide-volume studies between those using Mars Orbiter Laser Altimeter (MOLA) dataset at ~450 m/pix or HRSC at 50-200 m/pix and those using HiRISE data at 1-2 m/pix, which is only partially filled by CTX elevation data at ~20 m/pix. The CaSSIS camera on board the ESA/Trace Gas Obiter (TGO) can be used to produce DEMs, but so far, such data have not yet been used to conduct a landslide volume analysis. Here, we use three reconstruction methods (semi-automatic, morphology-based and tilted) on a CaSSIS DEM to estimate the initial topography and hence the volume and the distribution of erosion and deposition of a 6 km long landslide in Baetis Chaos. Despite the complex topography of the surrounding area due to the presence of an ejecta deposit beneath the landslide, we were able to estimate the landslide's volume and mass distribution. Using a tilted plane as part of estimating the initial topography produced the best results. We evaluated the success by considering the quantifiable balance between erosion and deposition (given the uncertainties) and more subjectively by considering whether the volume distribution matched with what was expected based on the morphology in images alone. Therefore, we recommend the use of this method for individual landslide studies in complex topography where detailed knowledge of the deposit-thickness distribution is required. The semi-automatic reconstruction method produces satisfactory volume estimates and would be better suited to studies where hundreds of landslides are present. We found that CaSSIS data can be used to successfully conduct such analyses, providing additional DEM coverage to study martian medium-scale landslides or other landforms of similar scale (5-15 km) with the notable benefit that it provides single-pass stereo image acquisition.

1. Introduction

Martian landslides are common features that can have morphologies that resemble Earth debris slides (e.g., Crosta et al., 2018), mudflows (Guimpier et al., 2021), or giant rock avalanches (McEwen, 1989; Quantin et al., 2004; Magnarini et al., 2019). They can mobilise large quantities of material up to 10^{12} m^3 and spread over areas of up to 10^9 m^2 (Quantin et al., 2004; Crosta et al., 2018b). The typical morphology of a landslide is composed of three distinct zones (Highland and Bobrowsky, 2008): the erosion zone at the top of the landslide, the transport zone through which the material transits and the deposition zone where the material accumulates.

In order to better understand the dynamics of landslide formation, it is important to quantify the volume of mobilised material and understand both the distribution and thickness of the deposit. The dynamics of landslides can be influenced by parameters such as the presence of water or ice within the sliding material (Cruden and Varnes, 1996), so a better understanding of their dynamics permits a better understanding of the conditions in which these landslides are formed. When compared with the vertical and horizontal distances travelled, the volume of the sliding mass can be used as a measure of the event mobility and used to compare it to other landslide events (Lucas and Mangeney, 2007). Moreover, the mass distribution of the deposit can be compared with the outputs of 3D flow simulations of landslides (Crosta et al., 2018b; Magnarini et al., 2019; Guimpier et al., 2021; Pajola et al., 2022), which can be used to better understand the physical mechanisms involved in the mass movement. In the case of recent terrestrial landslides, these volume calculations can be obtained by differencing Digital Elevation Models (DEMs) from pre- and post-landslide (Tsutsui et al., 2007).

For places where no pre- landslide topographic data are available, a topographic reconstruction is needed to obtain a pre-landslide DEM. This kind of reconstruction is carried out on Earth when no pre-event topography exists, such as on volcanic events using a DEM with a spatial sampling of 5 m/pix (Rodriguez-Gonzalez et al., 2010) and on landslides using DEM with a 0.1-0.2 m vertical resolution and 2 m spatial sampling (Conoscenti et al., 2015).

On Mars, topographic reconstruction has been carried out for landslides using the Mars Orbiter Laser Altimeter (MOLA) data, which has a 1.5-2 m vertical resolution (Quantin et al., 2004; Lucas and Mangeney, 2007; Lucas et al., 2011). However, because of the spatial sampling of 463 m/pix (Smith et al. 2001a) only landslides bigger than ten kilometres have been studied. Also, data from the High Resolution Stereo Camera (HRSC), which has a maximum of 10 m vertical resolution (Neukum et al., 2004), has been used for landslide reconstruction (Crosta et al., 2018b). These authors used HRSC DEMs with spatial sampling of 15 m/pix allowing the study of landslide < 10 km, yet the vertical resolution leads to significant uncertainty in the volume calculation for smaller landslides. Finally, elevation data from the High Resolution Imaging Science Experiment (HiRISE) with 1-2 m/pix spatial sampling and <1 m vertical resolution has been used to perform topographic reconstruction for kilometre-scale gullies (Conway and Balme, 2014; de Haas et al., 2015) and landslides (Guimpier et al., 2021; Pajola et al., 2022). However, features larger than 6 km cannot generally be accommodated in a single DEM due to relatively narrow HiRISE imaging swath (McEwen et al., 2007).

Out of the 3000 landslides identified on Mars (Crosta et al., 2013, 2018b), around 1/3 fall between these two spatial scales. The Colour and Stereo Surface Imaging System (CaSSIS) instrument on board the Trace Gas Orbiter (TGO) can be used to produce DEMs with a 4-5 m vertical resolution and 15 m/pix spatial sampling and have a spatial coverage of 9.4 by 47 km (Thomas et al., 2017). Such DEMs have never been used to perform topographic reconstruction of landslides, and together with CTX could be used to fill the scale-gap between HiRISE and HRSC-MOLA. The benefit of the CaSSIS camera over CTX is that it uses a 180° rotation mechanism to capture stereo images of a given site in a single pass (Thomas et al., 2017).

Our first aim is to test whether topographic reconstruction of a terrain is possible given the spatial sampling and quality of CaSSIS DEM data and to determine whether it is possible to derive useful information for the analysis of landslide dynamics (estimation of the volume and thickness of the deposit). For this purpose, we use a 6 km long landslide located in Baetis Chaos region where no stereo HiRISE nor exploitable stereo ConTeXt (CTX at 6 m/pix) imagery datasets are available. We then test three reconstruction methods to estimate the mass distribution and volume of the landslide with the aim to understand which method produces the best result.

In this manuscript, we first introduce previous methodologies used to reconstruct topography in landslide studies on Mars. Then we present the geographic context and the morphology of the landslide used in this study. Afterwards, we describe the methodology used to create the CaSSIS DEM followed by a description of the three reconstruction methods and associated uncertainties. Finally, we present the results of each reconstruction method and provide an assessment on the use of CaSSIS stereo data for pre-landslide reconstruction.

2. Brief summary of previously used topographic reconstruction methods

In order to better understand the dynamics of martian landslides, several studies have already been carried out that estimate landslide volumes or deposit distributions. In the following section, we will briefly review the different methods used to carry out these estimates. We first describe topographic reconstruction methods applied to large numbers of landslides in population-scale studies (Section 2.1) and then reconstruction methods applied at local scales for selected individual case studies (Section 2.2).

2.1. Martian landslide population-scale studies

Quantin et al. (2004) studied 45 large landslides within Valles Marineris (with volumes ranging between $5x10^{10}$ and $5x10^{12}$ m^3) and estimated the landslide volumes with two methods, one using the erosion zone of the landslides and another using the surface area of the deposit combined with an estimate of the height at the deposit front. For the second method, following Legros (2002), they multiplied the estimated volume by 7, because the toe of the deposit is not thought to be representative of the average deposit thickness. To estimate the volume of the erosion zone, Quantin et al. (2004) reconstructed its initial topography using two reference topographic profiles extracted from the MOLA

gridded data (with a 1.5-2 m vertical resolution and 463 m/pix spatial sampling), located on each side of the landslide to interpolate the pre-landslide topography. This method is quick to implement, but does not take into account local variations in topography specific to each landslide. Accordingly, they estimated expansion coefficients ranging from 5% to 70%, which have been calculated by taking the difference between the erosion zone volume and the total deposited volume (Fig.9 in Quantin et al., 2004). This coefficient should correspond to the decompaction of material induced by the mass movement processes (Chen et al., 2005). However, they interpret this wide range of values as mainly resulting from error during the pre-landslide reconstruction due to topographic irregularities, as in reality the expansion coefficient should not exceed 33% (Jaboyedoff et al., 2019). Their reconstruction method underestimates the deposition volume compared to the initial volume of the erosion zone due to inclusion of topographic irregularities under the deposits. Quantin et al. (2004) used their volume calculation to assess to the mobility of these landslides by comparing the coefficient of friction to the volume and then comparing those to terrestrial data.

Brunetti et al. (2014) studied 219 landslides in Valles Marineris and determined the volume of 49 of them, comprised between 10^7 and 10^{12} m^3. To determine these volumes the authors first mapped the landslide outline and used its geometry to reconstruct the geometry of the failure plane, they used both HRSC and CTX image data (with a spatial sampling of 15 m/pix and 6 m/pix, respectively) for landslide identification and used MOLA data at 463 m/pix for the topographic reconstruction. To take into account the uncertainties in estimating the failure plane position, they selected a deeper and a shallower surface based on the geomorphological and topographical constraints. They then computed the volumetric difference between the present-day topographic surface and the shallower and deeper surface. The landslide volume was then estimated by averaging the two volumetric differences leading to a maximum error in the volume estimation of a factor of two. Brunetti et al. (2014) compared their results to volumes of terrestrial landslides and found that the Valles Marineris landslides are similar to the largest submarine landslides on Earth. Using their volume calculation, they also derived an empirical relationship between the volume of the landslide and its area. They used this empirical relationship to estimate the volume of 83 landslides classified as rock slides and complex/compound landslides for which they did not undertake a reconstruction.

Crosta et al. (2018b) classified the morphology of 3118 martian landslides located between 60°N and 60°S. For 222 of these landslides, they estimated their volume using HRSC data for 74% of the landslides (maximum 10 m vertical resolution, 15 m/pix spatial sampling) and MOLA data for the remaining 26%. In order to manually reconstruct the initial topography of the landslide, which is required to estimate the volume of the deposit and of the erosion zones, they extrapolate the neighbouring topography within the landslide by drawing contour lines with maximum 50 m interval. They find volumes between 10^7 and 10^{12} m^3, and estimate the mean error of the volume calculation to be about 40%. This value results from the difference between the maximum and minimum volume calculated by least square fit on the volumes of 222 martian landslides divided the average volume for each landslide (Crosta et al., 2018a). They used these volume calculations to establish a relationship between the mean volume of the landslide and the area of the deposit. Then, by using the Heim's ratio, i.e., the ratio between the vertical drop height (*H*) and the horizontal runout distance (*L*) they estimated the landslide mobility and found a dependency with the landslide volume: the higher the landslide volume, the higher the landslide's mobility. Using their relationship between the mean volume and the landslide deposit area for the 222 cases, they apply this relationship to the remaining 2896 landslides in their database to estimate their volumes (Crosta et al., 2018a).

2.2. Individual landslide studies

Lucas et al. (2011) focussed on four landslides in Valles Marineris which they estimated to have a volume between 10^8 and 10^{11} m^3 using MOLA data (with a 1.5-2 m vertical resolution and 463 m/pix spatial sampling). They used two main steps to reconstruct the pre-landslide topography. First, they removed the topographic data in the deposit zone and manually reconstructed the contour lines in the deposit zone. They then interpolated the elevation values using the reconstructed contours using a kriging algorithm (Stein et al., 2002), which takes the spatial position and the spatial variability of the

topographic information into account. Then, they reconstructed the topography of the erosion zone using the surrounding topography to connect each side of the contour line across the erosion zone– they used three different initial shapes for the sliding surface which extends under the deposits. They determined the expansion coefficient for each landslide, ranging between 9% and 70%, with +/-10% as a margin of error. They stated that the 70% expansion coefficient could be a result of reconstruction error and/or be a real signal resulting from a greater dilatancy of the material during its deposition compared to the other landslides. The aim of this study was to determine the influence of the shape of the sliding surface in the erosion zone on the flow dynamics of landslides using numerical simulations.

Magnarini et al. (2019) focused on a landslide located in Coprates Chasma in Valles Marineris of more than 50 km long and 60 km wide. They did not estimate the volume of the landslide, instead, they used the thickness of the deposit to study the longitudinal ridge distribution on the landslide. They used CTX-derived DEM with a vertical resolution between 2 and 13 m and about 15 m/pix spatial sampling. To perform the pre-landslide reconstruction, they extrapolate the contour lines located outside the landslide into the landslide's interior. Then, they estimated the error on the landslide deposit thickness to be between 25 and 70 m which is consistent with the local magnitude of topographic variation of 80 m. Magnarini et al. (2019) found that the wavelength of the longitudinal ridges is 2-3 times the average thickness of the deposit.

Guimpier et al. (2021) described and reconstructed the pre-landslide topography for three small landslides in the Nilosyrtis Mensae region, with a volume less than 10^7 m^3. A similar reconstruction process was also used in Pajola et al. (2022). These two studies used HiRISE DEM data, with 1 m vertical resolution and 1-2 m/pix spatial sampling. In these studies, both of the volume and thickness of landslide were calculated and used for analysis. To perform the reconstruction, they used the DEM to derive elevation contours of each landslide at 25 m interval. After delimiting the landslide boundary, they manually reconstructed the topographic contour lines inside the landslide boundary, using the shape of the topographic contour lines outside the landslide boundary as a guide. These new reconstructed contour lines are then converted into point features at 2 m interval and then interpolated into a DEM using the Natural Neighbour algorithm (e.g., Watson, 1999) to obtain the reconstructed initial topography.

2.3 Summary

Most of the martian landslide studies have used topographic reconstruction techniques to estimate the volume of landslide in order to analyse the mobility of the landslides and to compare them to terrestrial analogues. In some cases, detailed studies are performed that analyse the volume and thickness of the deposits in order to examine specific aspects of landslide dynamics (e.g., Quantin et al., 2004; Lucas, 2010; Lucas et al., 2014; Brunetti et al., 2014; Magnarini et al., 2019; Guimpier et al., 2021).

To reconstruct the initial topography, most of the methods used so far in the literature exploit topographic contour lines derived from a DEM. In our study, the three reconstruction methods use this same starting point. Different adjustments are applied to produce the best landslide volume and thickness estimations.

3. Overview of the study area

The study area is located in Baetis Chaos (0°14' S, 60°34' W) (*Fig.1a, b*). Martian chaos terrains were first described by Sharp (1973) and they are commonly characterised by a rough floor topography where irregular jumble of blocks with different sizes occur (ranging from hundreds of metres to several kilometres in size). These blocks, generally have a fairly flat top-surface, flanked by steep slopes and can reach several kilometres in diameter (e.g., Pajola et al., 2016). The exact formation mechanism of chaos terrain in general is still under debate and in the case of Baetis Chaos the following hypothesis has been put forward. Located to the northwest of Juventae Chasma and connected in its northern part to Maja Valles, Baetis Chaos is thought to be formed through a deep fluvial incision after a

catastrophic flooding of ancient lake in Juventae Chasma (Coleman and Baker, 2009), which is thought to have occurred during the early Hesperian (3.33 Ga) (Gross et al., 2009). As a result, Baetis Chaos appears as a 55 km wide and 75 Km long north-south oriented oblate depression with a depth of 700 m (*Fig.1b)*, containing numerous chaos blocks. The area has a relatively abrupt southern escarpment and at its northern end it shallows gradually into the Maja Valles outflow system. The geologic map of Tanaka et al. (2014) classifies this region as part of a Middle Noachian highland unit. Indeed, it is mostly composed of moderately to heavily degraded undifferentiated impact, volcanic, fluvial and basin materials (Tanaka et al., 2014).

On the southern escarpment of Baetis Chaos there are four north-facing landslides located 1200 m above the martian reference level (*Fig.1b*). The landslide deposits are located on the Chaos floor and cover the ejecta of a 13 km diameter impact crater located 5 km to the southwest (*Fig.1c*). Hence, the landslides are younger than the ejecta they cover. These ejecta deposits have a complex surface roughness which may have influenced the emplacement of the landslides.

We focus in this study on the easternmost of these landslides which measures ~6 km long and 3.4 km at its widest point (*Fig.1c)*. The other landslides are only partially covered by the available CaSSIS stereo data, hence we decided to not focus on them. We divide this landslide into three distinct areas, the erosion zone, the transport zone and the deposit zone (*Fig.1c, d*). The erosion zone is located at the top of the landslide, it cuts into the plateau bounding the southern edge of Baetis Chaos and it is characterised by a well-defined erosion scar. There is residual material at the base of the erosion zone comprised of a flat area, which appears to be a displaced, yet practically intact, portion of the plateau (*Black arrow, fig.1b, c*). The slope of the erosion zone reaches 35° and becomes almost flat (2°) where the residual material is located. The erosion zone is followed by the transport zone with a 28° inclination. The deposit zone covers the impact crater ejecta and therefore is hummocky in appearance because of the ejecta roughness, but slopes at ~3° towards the north direction at the hundred-metre scale.

4. Methodology

In order to perform the pre-landslide topographic reconstruction, we need a post-landslide DEM of the area within which the landslide is clearly recognisable (which is not the case for MOLA or HRSC). CaSSIS provides a more detailed representation of this landslide and allows, with its stereo capability, a more complete analysis than could be performed with the other existing data (Fig.3b). In section 4.1., we detail the DEM construction from the CaSSIS stereo images using 3DPD (three Dimensional reconstruction of Planetary Data) software (Simioni et al., 2021) and we then explain the three different methods used to reconstruct the pre-landslide topography with this CaSSIS DEM in section 4.2.

246

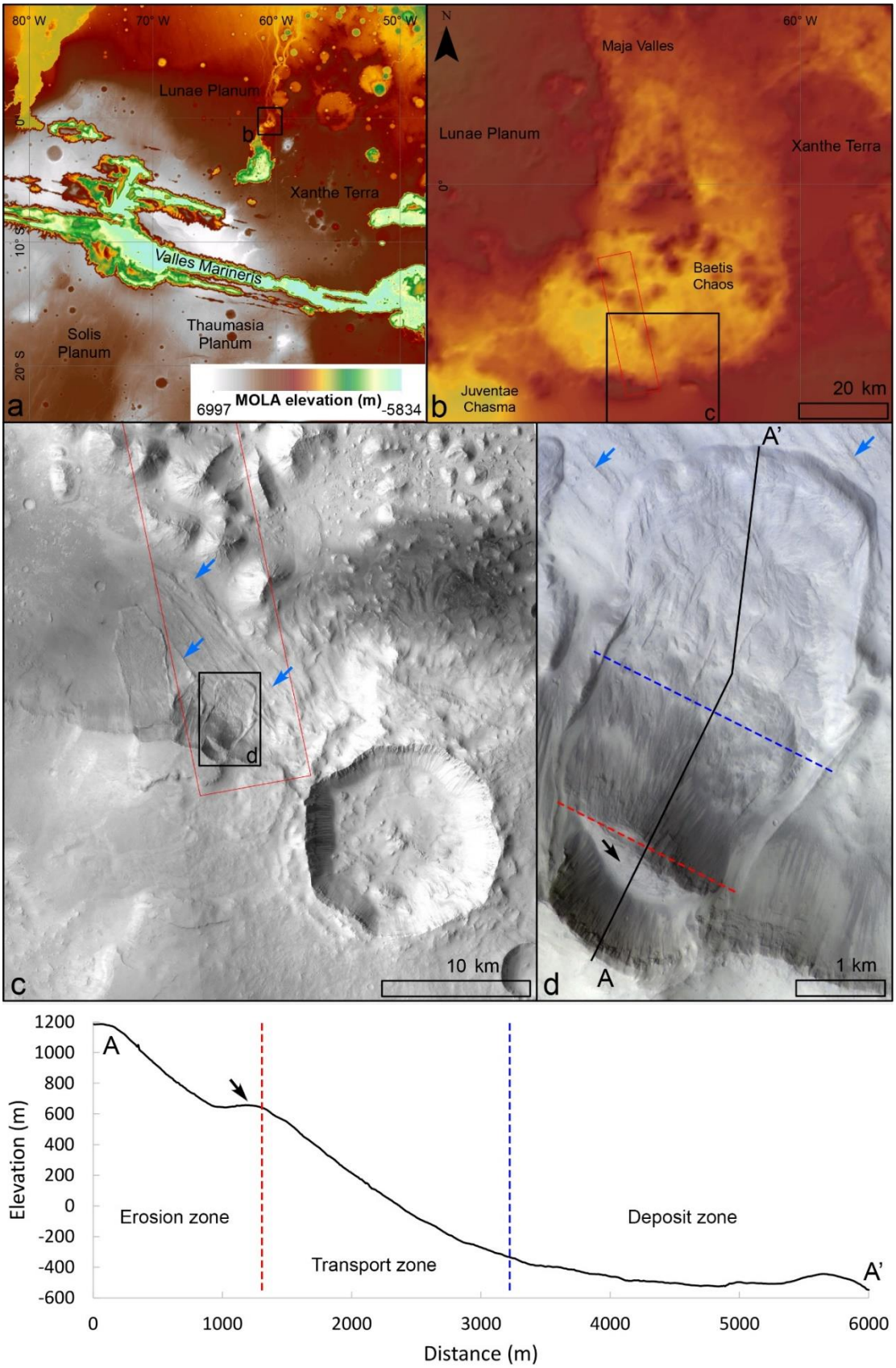


Figure 1 – (a) Colour representation of the MOLA DEM indicating the location of the study area (North of Valles Marineris); (b) The MOLA DEM in the Baetis Chaos region; (c) CTX images of the study area in Baetis Chaos, blue arrows indicate raised ridges due to the ejecta of the crater in the SE part of the image (F04_037533_1813, J15_050746_1774); (d) Detailed view of the landslide. The black arrow indicates the residual material in the erosion zone, while blue arrows indicate raised ridges due to ejecta (CaSSIS image MY34_005367_181_1, RED, PAN, BLU filters, image footprint marked in red in panels (b) and (c)); (e) Longitudinal profile of Baetis landslide using a CaSSIS DEM. Credits: NASA/JPL/MSSS/UofA/ESA/Roscosmos/UniBe.

4.1. DEM creation

On the landslide study area (*Fig.1b*), we planned and acquired a CaSSIS stereo pair (*Fig.2*) characterised by a spatial sampling of 4.6 m/pixel (*Table 1*).

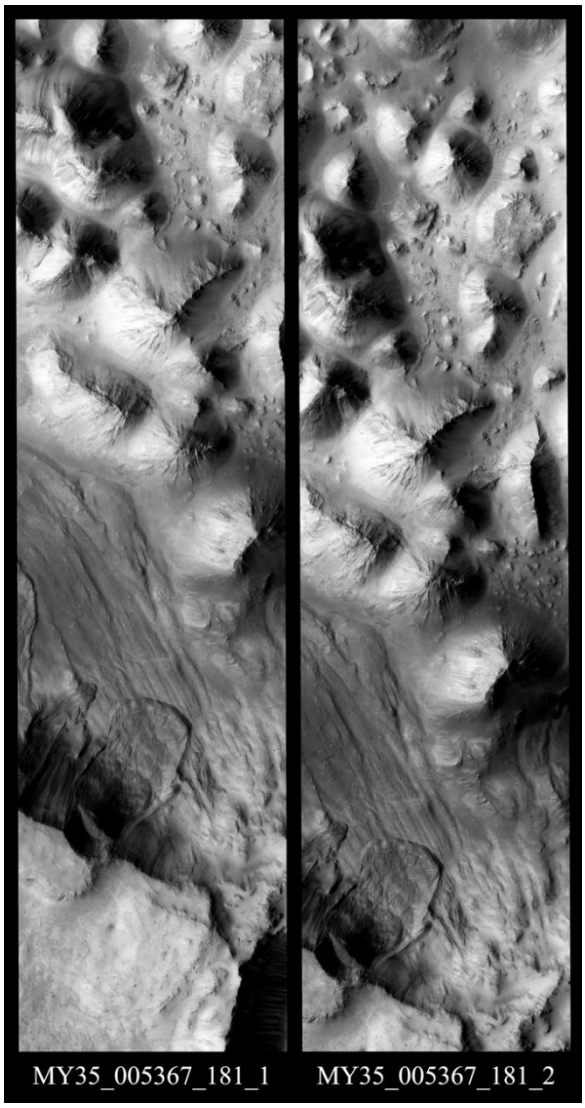


Figure 2 – The CaSSIS stereo pair acquired (PAN channel). The landslide under study is located in the bottom part of the image. Credit: ESA/Roscosmos/Unibe.

In order to construct the CaSSIS DEM, we used the 3Dimensional reconstruction of Planetary Data (3DPD) photogrammetric pipeline described in Simioni et al. (2021), and summarised here, the pipeline demonstrated an accuracy comparable to well-known ASP pipeline (commonly used for CTX images) (Re et al., 2019).

First, the framelets were mosaicked into a single image making use of the attached Spice Kernels (Acton, 1996). Such framelets are already radiometrically calibrated (Thomas et al., 2022). The geometric calibration is applied while mosaicking, and the bundle adjustment process consequently returns the best undistorted panchromatic images. The images are then rectified projecting them on a plane at a height derived through the intersection of the boresight direction with the MOLA surface (Smith et al., 2001). The matching workflow then focuses on a feature-based extraction of the seed points that are used for finding sparse disparity, extrapolated to the full image. Consequently, through the Delaunay triangulation (Chew, 1989) the starting location of the matching pairs are determined and an approximate parallax field is defined. A Normalised Cross Correlation (NCC, Lewis, 1994) pyramidal coarse-to-fine algorithm is performed to reduce the search area and to limit blunders. Finally, after the application of a 2D parabola fit, a Least Squares Matching (LSM) algorithm (Gruen, 1985) is used to refine the disparity map, and the final projected product (ID CAS-DTM-MY34_005367_181_1-OPD-01-02) is obtained (*Fig.3a*).

CaSSIS Image ID	MY35_005367_181_1	MY35_005367_181_2
Local Time	15:26:34	15:27:24
Incidence Angle (°)	52.297	52.497
Emission Angle (°)	10.959	11.016
Phase Angle (°)	51.285	51.109
Pixel Scale (m)	4.6	4.6
Filters Acquired	PAN – RED – BLU	PAN – NIR – BLU
Convergence angle (°)	22.4	

Table 1 – Details of the CaSSIS images acquired and used to generate the DEM used in this analysis.

4.2. Reconstruction of the initial topography

In order to estimate the mass distribution and the volume of the landslide, we need to reconstruct the initial topography before the Baetis Chaos landslide occurred. Using the DEM we adapt the method

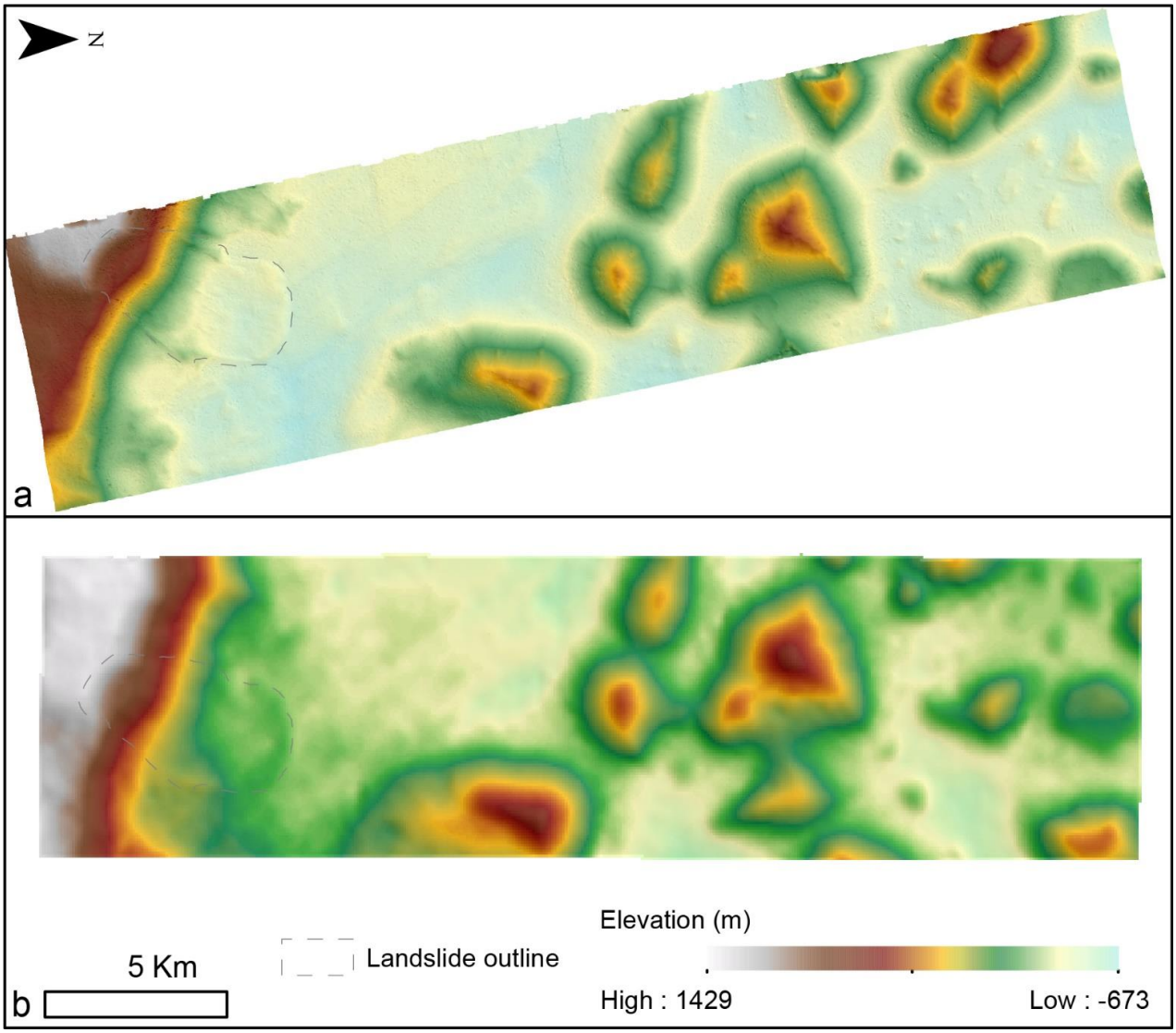


Figure 3 – (a) Colour-keyed rendering of CaSSIS DEM with semi-transparent hillshade (MY34_005367_181) compared to (b) the standard HRSC DEM product displayed with the same elevation colours (h1059_0000) Credits: ESA/DLR/FU Berlin/Roscosmos/INAF

used in Conway and Balme (2014) and de Haas et al (2015) using three levels of complexity to test the fidelity of each reconstruction: i) a semi-automatic method; ii) a manual method that is informed by the morphology of the terrain surrounding the landslide; and iii) a manual method that is informed by the morphology of the terrain surrounding the landslide and applies a terrain tilt to improve the reconstruction of the deposits. Each additional step should represent an improved, better reconstruction, but as the complexity increases, the computation time does as well, from a few minutes with method 1 to several hours with method 3. For each reconstruction method, we estimate the uncertainties linked to the data and to the reconstruction procedure and these calculations will be described at the end of the methodology section.

Before starting any further processing, in order to remove artefacts produced during the DEM creation (see supplementary material), we first smooth the DEM, by applying a 10-cell radius moving average. For each reconstruction method, we start by deriving the contour lines from the DEM at a 25 m interval. Then, we digitise the outline of the landslide by identifying sudden changes in the contours correlated with textural changes along the boundary of the landslide. We also made use of a second outline which we call the “reconstruction outline”, which is located outside the original outline at a maximum distance of 300 m, hence excluding any possible topographic feature related to secondary processes that may have degraded the landslide. We placed the reconstruction outline at the point just before the contour lines start to curve as they encounter the landslide outline.

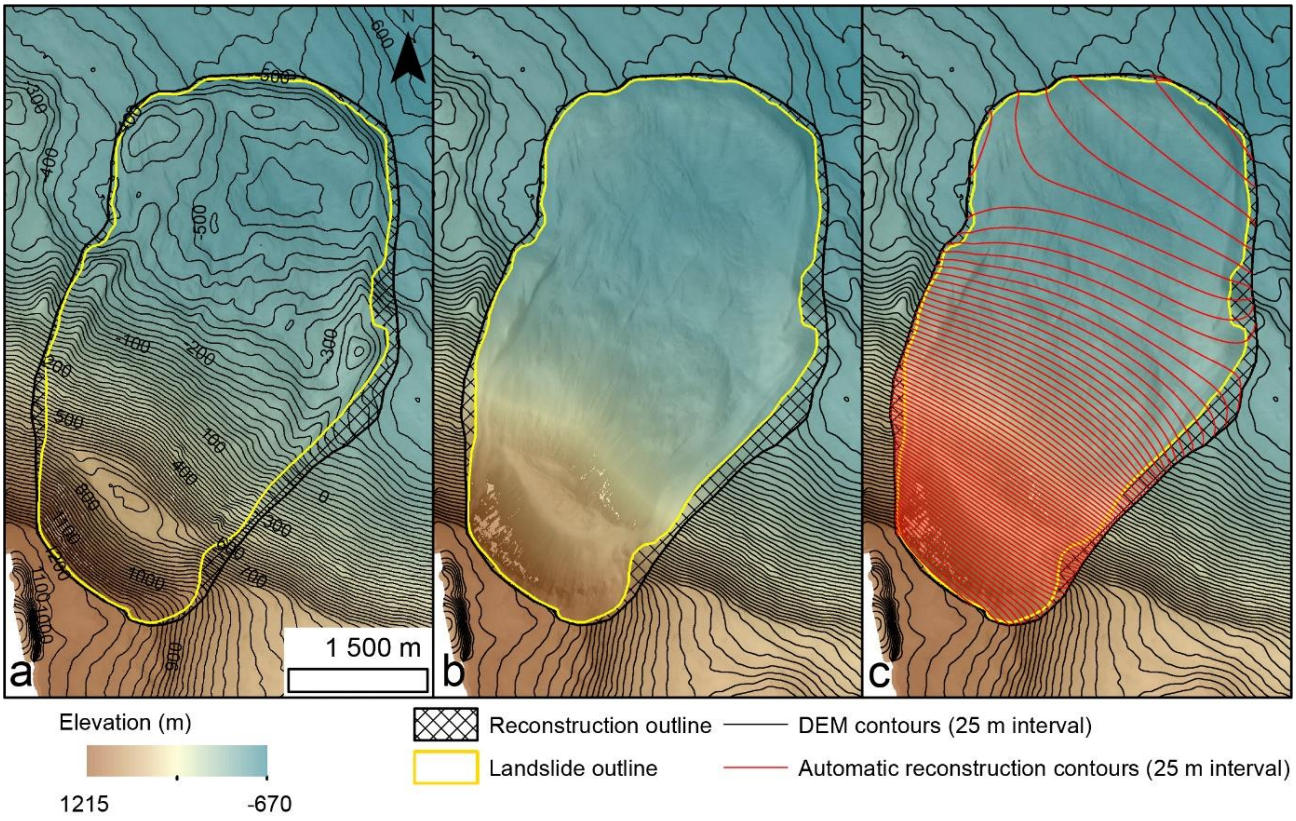


Figure 4 – Key steps in the semi-automatic reconstruction method (a) Colour-coded original CaSSIS DEM of Baetis Chaos landslide with contour lines at 25-m interval overlain by the semi-transparent PAN orthoimage. (b) Same as panel a without the contour lines inside the landslide reconstruction outline. (c) Automatically reconstructed contour lines in red produced from a DEM interpolated using the Natural Neighbour interpolation algorithm. Credit: ESA/Roscosmos/Unibe/INAF

Semi-automatic method. The semi-automatic method uses minimal manual intervention and an interpolation algorithm to allow fast reconstruction of the initial topography. First, we remove the contour lines inside the reconstruction outline (*Fig.*4a & b). We convert the contour lines outside the reconstruction outline into feature points containing elevation data every 2 m. Then, we fill this gap using the Natural Neighbour interpolation algorithm (e.g., Watson, 1999) to produce a new DEM without the landslide (*Fig.4c*).

A final smoothing step is applied to remove artefacts that can be created by the interpolation on the DEM. For each DEM cell, we average the elevation values within a 10-cell radius around a central cell. We defined this value on the basis of the size of the artefacts identified on the original DEM.

Morphology-based reconstruction method. This reconstruction method is based on a manual reconstruction informed by the topography around the landslide, followed by interpolation. As before, we remove the contours inside the reconstruction outline. With this method, we manually reconstruct the contour lines inside the reconstruction outline using the topographic contour lines outside the landslide outline as a guide (Fig.5b). In addition, we used the morphological characteristics of the landslide to better estimate the initial shape of the erosion zone. By using the CaSSIS images, coupled with the longitudinal profile (*Fig.1d, e*), we observed that the residual material in the erosion zone has a flat surface. This suggests that it is an intact portion of the plateau above. Hence, we use the topography of this residual material (Fig.5a, green contour lines) to better reconstruct the upper part of the erosion zone, as follows. We manually shift the contour lines of the residual material (*Fig.5b, blue contour lines*) to place them at the top of the erosion zone. We then connect the contour lines of the residual material smoothly into the surrounding topographic contour lines and replace their elevation values with those of the surrounding contours.

For the rest of the landslide, we manually connect the ends of the corresponding contour lines located on either side of the landslide guided by their curvature outside the landslide (*Fig.5b, red contour lines*).

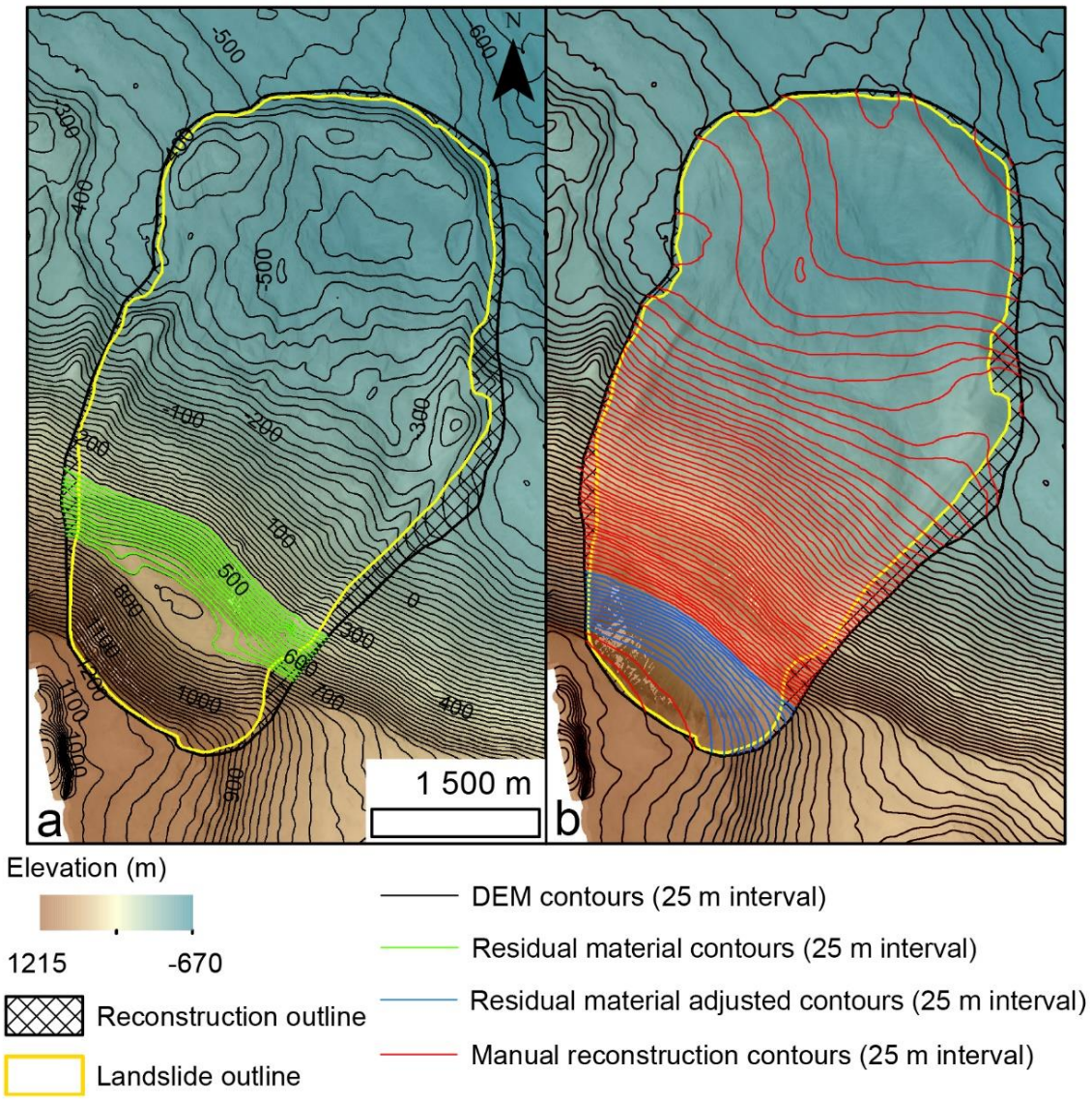


Figure 5 – Key steps in the morphology-based reconstruction method. Background is the colour-coded CaSSIS DEM with semi-transparent PAN orthoimage. (a) CaSSIS DEM contour lines with 25-m interval in black. The residual material is in green. (b) Manually reconstructed contour lines in red inside the reconstruction outline. The shifted and merged residual material contour lines appear in blue. Credit: ESA/Roscosmos/Unibe/INAF

The final step is to create the new DEM by converting the contour lines into points every 2 m containing elevation data. Afterwards, we interpolate them using the Natural Neighbour interpolation algorithm, as for the previous method. To remove artefacts at the interface between surrounding topography and manual reconstruction, we used the same smoothing method as described above.

Tilted reconstruction method. This final reconstruction method increases the number of contours on the deposit zone. In the previous method, there are few contour lines on the deposit zone, this means that details are missing in this zone. As shown in *figure 1a*, the chaos floor is covered by the ejecta deposit coming from the impact crater located to the southwest, and superposed by the landslide deposit. Given the irregularities observed on the chaos floor, the reconstruction of the landslide deposit zone could lead to an overestimation of the thickness and volume of the landslide deposit itself, if the ejecta deposits are not taken into account during the reconstruction process. To better reproduce the complexity of the initial topography of the chaos floor, we tilt the DEM prior to the reconstruction. This additional step, reduces the amplitude of the irregularities expressed by the contours (making them easier to project) and increases the number of contour lines for the same contour interval, therefore providing more information into the final interpolation.

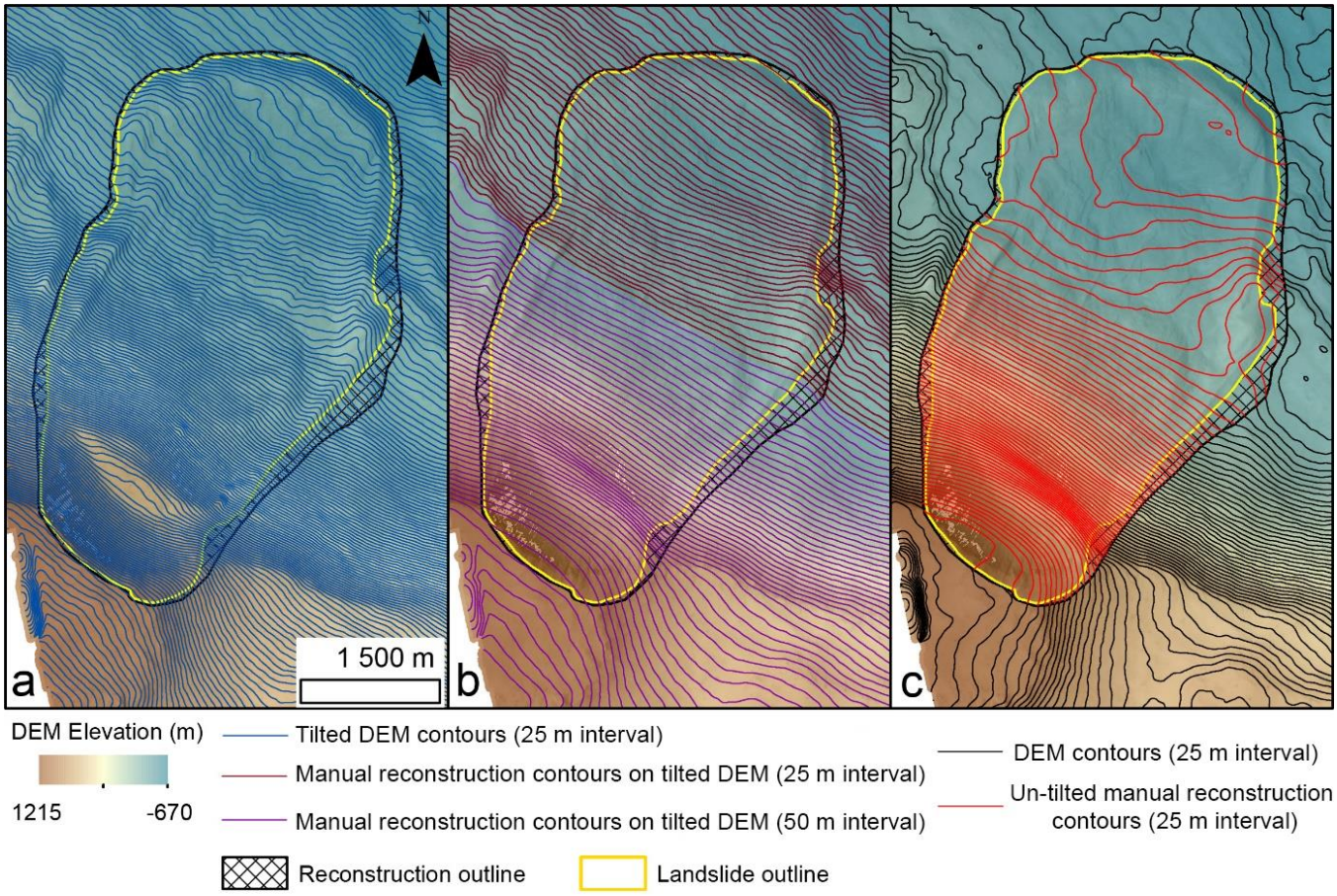


Figure 6 – Key steps in the tilted reconstruction method. Background is the colour-coded CaSSIS DEM with semi-transparent PAN orthoimage. (a) Contour line on a 15° inclined original CaSSIS DEM at 25-m interval. (b) Manually reconstructed contour lines on the 15° inclined DEM at 25-m interval in brown for the deposit zone and at 50-m interval in purple for the erosion and transport zones. (c) Contour lines of the reconstructed topography in red after removing the tilt.

To create this inclined plane, we draw a base line with a 0-metre elevation on the top of the erosion zone, perpendicular to downslope direction. From this baseline, we calculate the distance which we use to construct an inclined plane at 15° covering the entire landslide. This angle was chosen in order to provide a sufficient number of contours without completely subduing the surrounding topography. We then subtract the inclined plane from the original DEM, to tilt it.

Using this tilted DEM, we derive contour lines at 25 m interval in the deposit area (*Fig.6a, brown contour lines)* and at 50 m interval for the erosion and transport area (*Fig.6a, purple contour lines*). We chose to increase the contour line interval to 50 m in the erosion and transport zone to avoid an excessive number of contour lines which would increase the time taken to manually connect them. Then, we proceed as for the previous method and manually replace the contours within the reconstruction outline (*Fig.6b*). We then convert the new contour line to points at 2 m intervals containing elevation data and interpolate them using the Natural Neighbour algorithm to create a reconstructed and tilted DEM. As before, we smooth the resulting DEM. Finally, we remove the tilt by adding the inclined plane to tilted DEM (*Fig.6c*).

4.3. Reliability of the methods

In order to estimate the reliability of each reconstruction method, we compare the volume of the erosion and deposit zone to determine the mass balance. In terrestrial landslides there is usually an expansion coefficient which corresponds to the decompaction of material induced by the mass movement processes (Chen et al., 2005; Pajola et al., 2022). Analysis of terrestrial landslides have shown that this expansion coefficient should not exceed 30% to 33% between the erosion and deposit volume (Jaboyedoff et al., 2019).

To estimate the landslide volume, we subtract the three reconstructed DEMs from the original DEM, hence obtaining three thickness maps of the landslide. The positive values of the thickness map correspond to deposition and negative values to erosion. By summing each positive or negative cell value and multiplying it by the cellsize, we obtained the volume of deposit and erosion zones, respectively.

4.4. Uncertainties

There are three main types of uncertainty related to this analysis. The first is related to the vertical accuracy of the DEM used and the second is related to the uncertainty in reconstructing an unknown initial topography. The third is related to the manual digitisation steps (tracing the outline of the landslide and the contours in methods 2 and 3).

The uncertainty related to the vertical accuracy (*Acc*) of the data is calculated using the method of (Okubo, 2010). We used the angle of convergence of stereo images of $\alpha = 22.4°$ (Thomas et al., 2017), the image resolution (*R, Table 1*) and assuming pixel correlation $P_{corr} = 1/5$ (Okubo, 2010) to estimate the vertical accuracy of the CaSSIS DEM using the following equation:

$$Acc = \frac{R \times P_{corr}}{\tan \alpha} \quad (1)$$

Using equation (1) we estimate the vertical accuracy to 2.23 m. In order to calculate the uncertainty of the deposit and erosion volume we multiplied their respective areas by 2.2 m providing a worse-case uncertainty value (presented in *Table 2*).

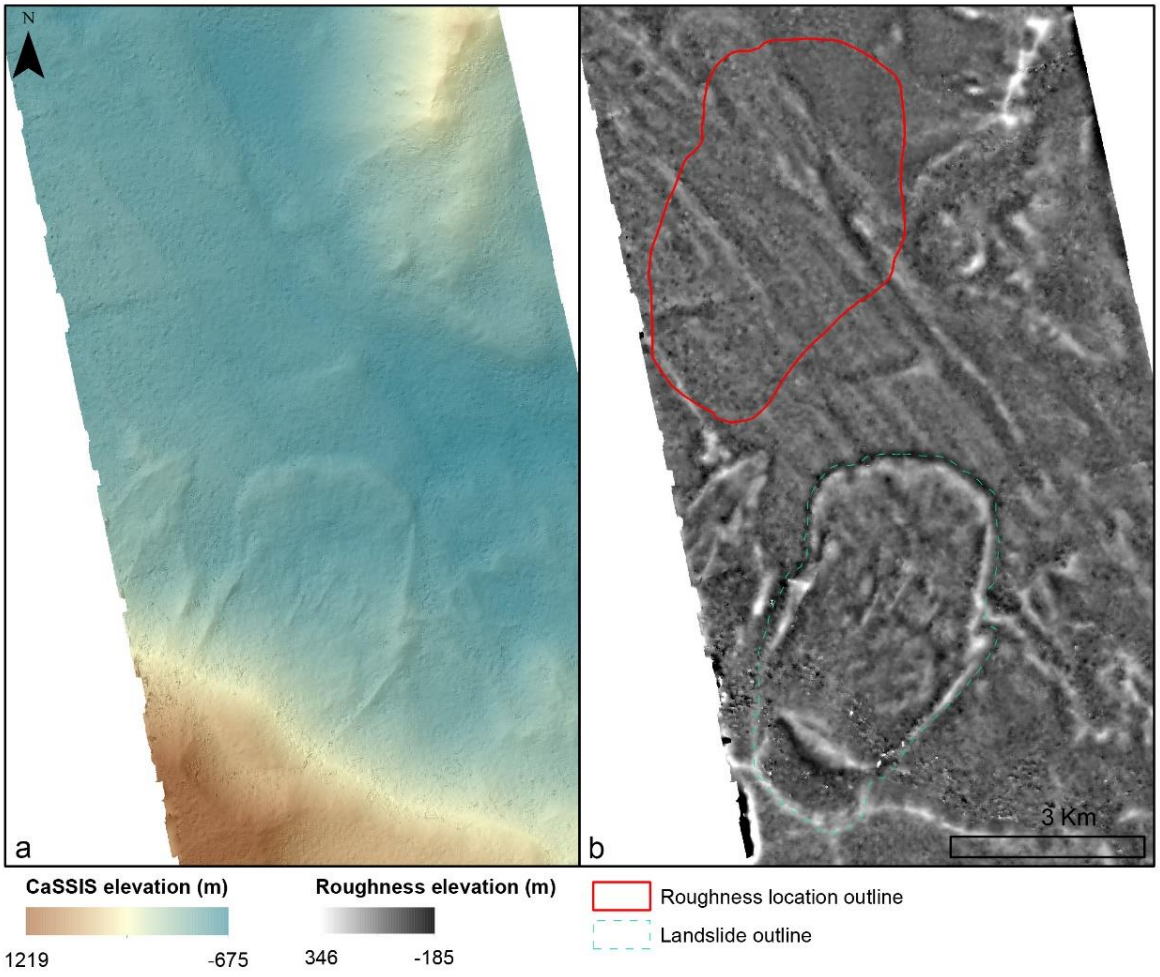


Figure 7 – (a) Colour-keyed CaSSIS DEM with semi-transparent PAN orthoimage MY34_005367_181_1 and the landslide location; (b) Roughness of the DTM showing the influence of the impact crater ejecta (See section 4.4 for details on how this was calculated). The red outline shows the area that was used to provide an estimate of the potential roughness of the surface before the landslide occurred for the uncertainty estimations. Credit: ESA/Roscosmos/Unibe.

The second uncertainty is related to the unknown topography of the area preceding the formation of the landslide. In order to quantify the likely magnitude of this uncertainty, we make the assumption that the terrain pre-landslide had a similar roughness to the undisturbed neighbouring terrain of this area. Hence, we sampled an area of the DEM not influenced by the landslide and whose surface is representative of the general roughness of the area (*Fig.7*). In this case, the majority of the topographic variation at the decametre-to hundred-metre scale originates from the ejecta deposits from the impact crater located to the east of the landslide. To estimate the magnitude of the ejecta-related roughness, we smoothed the CaSSIS DEM by applying a 50-cell radius moving average which we then subtracted from the original DEM. An additional smoothing of 10-cell radius moving average is then applied to avoid the presence of artefacts related to the original DEM (see supplementary material). The positive and negative values of the DEM of difference are separately summed over a given area (deposition or erosion area) and the mean taken of their absolute values to provide the volumes given in *Table 2*.

The third source of uncertainty derives from the manual parts of the reconstruction methods. For the semi-automatic method, the manual step, which can influence the volume calculation, is the position of the landslide boundary. In order to estimate the sensitivity of the volume calculation to the position of this boundary we recalculated the volume using the inner boundary of the landslide instead of the outer one as an extreme case. The difference between this volume and the original volume is taken as the uncertainty in *Table 2*.

The morphology-based and tilted plane reconstruction methods both involve a manually placing contour lines. To estimate the sensitivity of the volume calculation to this uncertainty the manual contour line reconstruction step was repeated three times for each of the two reconstruction methods. The volume was then recalculated for each deposit and erosion zone for the two-reconstruction methods. We obtain three volumes: initial volume, the second volume and the third volume from each reconstruction (*Table 2*) and we calculate the standard deviation to represent the uncertainty on the reconstruction from the digitisation.

We take the maximum value of these three uncertainty values as the final uncertainty on our volume estimates.

5. Results

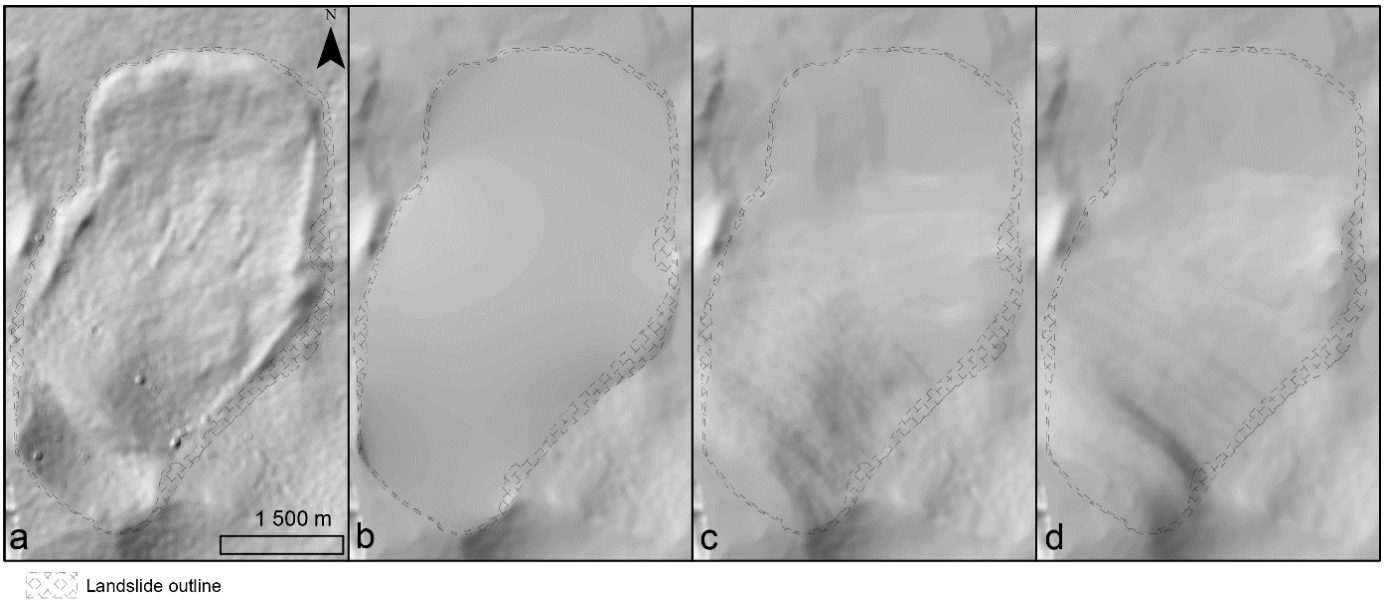


Figure 8 – Hillshaded relief view of (a) the original CaSSIS DEM with Baetis Chaos landslide. Hillshaded relief view of the topographic reconstructions using (b) the semi-automatic method, (c) the morphology-based method and (d) tilted method.

The three reconstruction methods provided different results, highlighting that the reconstruction is sensitive to the assumptions made during the reconstruction process and to the complex topography in the deposit zone. The ejecta deposits on the Chaos floor mean that the topographic reconstruction

414 is more uncertain if compared to the landslides that superpose the flat floor of Valles Marineris, for
415 example (e.g., Quantin et al., 2004).

416 The hillshaded relief view of the original and reconstructed DEM are shown in *Figure 8*. The elevation
417 difference map between the original DEM and each reconstructed DEM is shown on *Figure 9*. Then,
418 *Table 2* summarises the volume calculation for the erosion and deposit zones and the corresponding
419 expansion coefficient for each reconstruction. We describe below the results for each reconstruction
420 method.

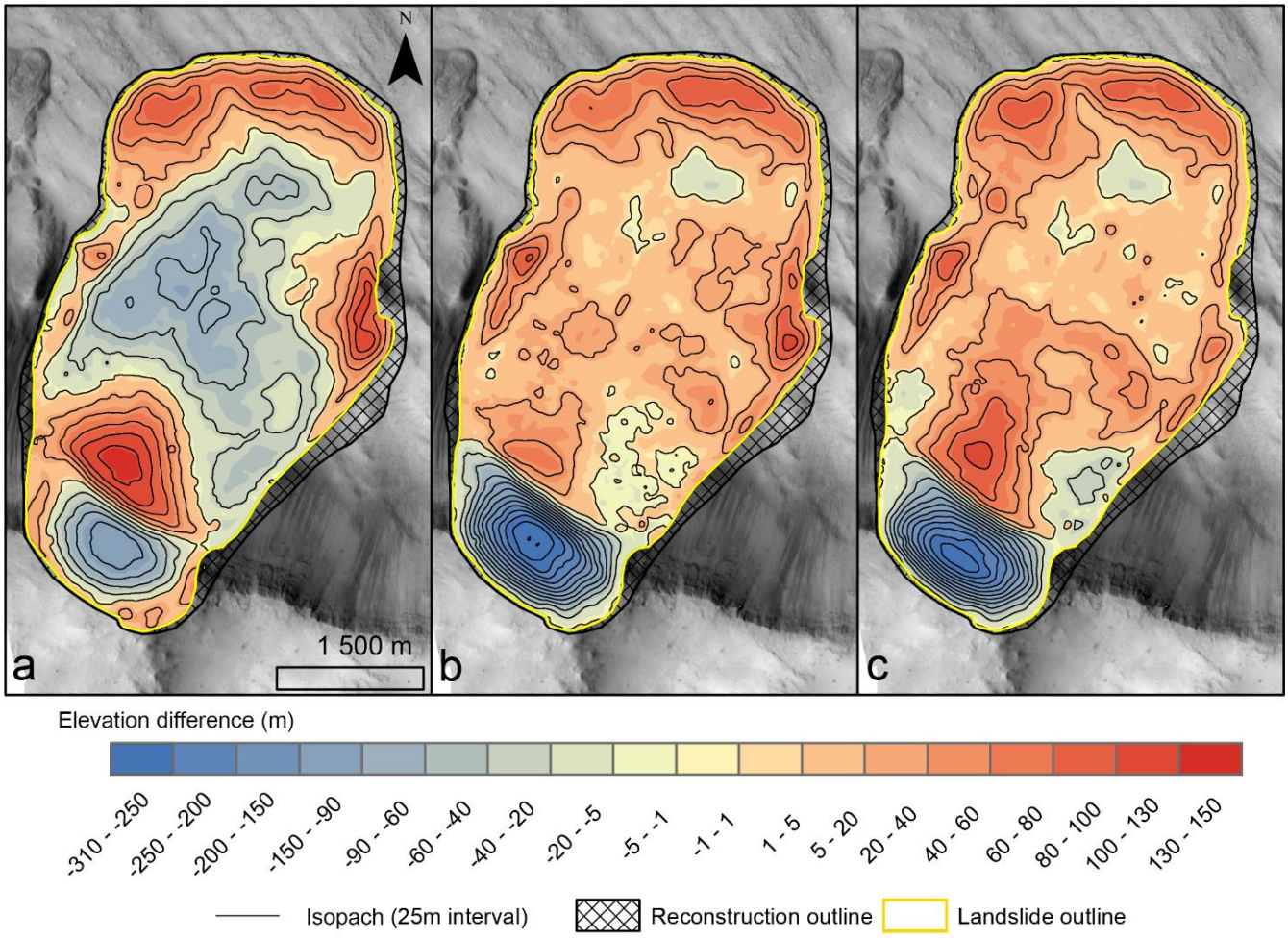


Figure 9 – Baetis Chaos landslide elevation difference using each reconstruction method with isopach lines at 25-m intervals. Background is the the CaSSIS PAN orthoimage. (a) The semi-automatic reconstruction method. (b) The morphology-based reconstruction method. (c) The tilted reconstruction method.

421 ***Semi-automatic method.*** This method was successful in removing the topographic signature of the
422 landslide, as shown by comparing the hillshaded relief view of reconstructed DEM (*Fig.8b*) with that of
423 the original DEM (*Fig.8a*). But even if we smooth the reconstructed DEM, there is an artificial step
424 visible around the landslide outline. In the elevation difference map of the landslide (*Fig.9a*), there are
425 two areas dominated by erosion: the first in the erosion zone with a maximum depth of 123 m and the
426 second spanning the transport and deposition zones of the landslide with a maximum depth of 93 m.
427 The second erosion area is not consistent with the visible surface morphology of the landslide which
428 does not indicate that any significant erosion has occurred in this area. This depositional part of the
429 landslide is mainly located at the front of the landslide and the eastern levee, with a maximum
430 thickness of 85 m, and deposition is also recorded for the residual material at the base of the main
431 erosion zone. We estimate the uncertainty on the eroded and deposited volume of 11% and 13%
432 respectively. The uncertainty related to the landslide digitisation dominates over the other sources of
433 uncertainty. This reconstruction method produces a smaller deposit volume compared to the erosion
434 volume resulting in an expansion coefficient of -9.0% (*Table 2*). By taking into account the uncertainty

435 on the volume calculation, the expansion coefficient could vary from minimum of -10.8% to maximum
436 of – 6.6% (*Table 2*).

		Semi-automatic method		Morphology-based method		Tilted method	
		Deposit	Erosion	Deposit	Erosion	Deposit	Erosion
Area (m^2)		$7.20x10^6$	$8.26x10^6$	$1.23x10^7$	$3.15x10^6$	$1.20x10^7$	$3.47x10^6$
Initial volume estimation (m^3)		$2.83x10^8$	$3.11x10^8$	3.2310^8	$2.38x10^8$	$3.59x10^8$	$3.22x10^8$
Vertical accuracy uncertainty	Percentage of the initial volume	6	6	8	3	7	2
	Volume equivalent to percentage (m^3)	$2x10^7$	$2x10^7$	$3x10^7$	$7x10^6$	$3x10^7$	$8x10^6$
Roughness uncertainty	Percentage of the initial volume	4	3	5	1	4	1
	Volume equivalent to percentage (m^3)	$1x10^7$	$1x10^7$	$2x10^7$	$3x10^6$	$2x10^7$	$4x10^6$
Outline/Contour uncertainty	Calculated volume n°2 (m^3)	$2x10^8$	$4x10^8$	$5x10^8$	$2x10^8$	$4x10^8$	$2x10^8$
	Calculated volume n°3 (m^3)	-	-	$4x10^8$	$2x10^8$	$4x10^8$	$3x10^8$
	Volume standard deviation (m^3)	$3x10^7$	$4x10^7$	$6x10^7$	$4x10^6$	$3x10^7$	$4x10^7$
	Standard deviation of percentage of initial volume	11	13	18	2	9	11
Expansion coefficient (%)		-9.0		35.7		11.5	
Expansion coefficient min (%)		-10.8		13.9		7.5	
Expansion coefficient max (%)		-6.6		56.3		16.7	

437 *Table 2 – Initial volumes of the erosion and deposit zone calculated for each reconstruction method with the associated*
438 *uncertainy volumes and the corresponding coefficient of expansion (calculated as: 100 x (deposition – erosion) / erosion).*

439 ***Morphology-based reconstruction method.*** This method also successfully removed the topographic
440 signature of the landslide (compare *Figs.8a* and 8c). In addition, there is a smooth transition between
441 the landslide and the surrounding topography (unlike for the previous method).

442 The elevation difference map (*Fig.9b*) reveals a distinct erosion zone at the top of the landslide
443 followed by a distinct deposit zone covering the last 4/5 of the landslide. The erosion zone has a
444 maximum depth of 300 m. The residual material at the base of the erosion zone has a maximum

thickness of 70 m, which is displaced to the west. The deposits are otherwise concentrated in the lateral levees whose thickness attains 110 m, while the toe of the landslide where the deposit is up to 95 m thick. The uncertainty estimate for this reconstruction method is 18% and 3% for deposit and erosion zones respectively. The vertical accuracy of the DEM dominates the uncertainty of the erosion zone, whereas the digitisation uncertainty dominates for the deposit zone (*Table 2*).

The volume calculation for erosion and deposit zone (*Table 2*) shows an expansion coefficient of 35.7% between the erosion zone and deposit zone. Taking into account the uncertainty for the deposit and the erosion zone volumes, we determined that the expansion coefficient could be between 13.9% and a maximum of 56.3% (*Table 2*). Hence, this reconstruction seems more consistent with the morphology of the landslide when compared to the semi-automatic method, even if the deposition volume appears to be overestimated.

Tilted reconstruction method. This method also successfully removed the topographic signature of the landslide (compare *Figs. 8*a and 8d) as it was the case for the morphology-based reconstruction method. Moreover, there is a smooth transition between the landslide and the surrounding topography. The elevation difference map (*Fig.9*c) reveals a similar overall pattern to that of the morphology-based reconstruction method with some key differences:

- The residual material at the base of the erosion zone is more central and thicker – 110 m. It is flanked by two erosional areas (5 to 20 m deep) corresponding better to our expectation's morphology of the landslide.
- The deposits are concentrated more evenly along the toe of the landslide and not so much in the levees, yet with a similar maximum thickness of 88 m.
- The expansion coefficient is lower, at 11.5%.

For this last reconstruction method, the uncertainty on the volume estimates are 9% and 11% for the deposit and erosion zones, respectively. The uncertainty is dominated by the digitization.

Taking into account the volume uncertainty the expansion coefficient value could be between 7.5% and 16.7%.

Overall, given the distribution of material inside the landslide and the volume balance, the tilted reconstruction method is the most consistent with the morphological observations compared to the other two reconstructions of the Baetis Chaos landslide.

6. Discussion

6.1. Assessment of three reconstruction methods

The semi-automatic reconstruction method produces a similar estimate of the overall volume of the landslide to the other two methods despite producing an unrealistic volume distribution. Therefore, this quick method would be appropriate if only an estimate of the volume is required. However, if we remove the second unrealistic erosion zone, which is located in the transport and deposition zones, the expansion coefficient reaches about 344%, revealing that the amount of erosion in the erosion zone is greatly underestimated. This landslide's complex underlying topography consisting of a plateau, followed by a cliff and impact ejecta on the chaos floor is too complex to be accommodated by the semi-automatic reconstruction method. However, in case of a simpler underlying topography, such as a landslide located on a continuous smooth slope and without breaks in slope or significant underlying roughness, this method could be applied (Guimpier et al., 2021), hence generating reliable volume distributions. Moreover, this methodology has the advantage of being simple and quick to implement.

The morphology-based reconstruction method better accounts for the large-scale variations in topography of the landslide area, with a topographic profile with a break in slope to produce a more realistic distribution of volume. However, this method produces an imbalance between the erosion and deposition volumes with an expansion coefficient of 35.7%, exceeding what might be expected due to decompaction alone (Jaboyedoff et al., 2019). If we take into account the possible minimum

493 expansion coefficient which is 13.9%, this reconstruction method would fit within the decompaction
494 limit set by (Jaboyedoff et al., 2019), but considering the possible maximum expansion coefficient
495 (56.3%), there is a large uncertainty associated with this reconstruction.

496 The tilted reconstruction method produces the most realistic volume distribution and has a reasonable
497 expansion coefficient of 11.5%, with also reasonable minimum and maximum expansion coefficient
498 taking into account the uncertainties. This last method is more time-consuming than the two others,
499 but in the specific case where the terrain morphology is complex, it produces better results. The
500 distribution of volume corresponds better with what might be expected from the morphology alone.
501 We recommend that in areas of complex topography the morphology-based reconstruction method
502 should be attempted, followed by the tilted reconstruction method if the morphology-based
503 reconstruction has not produced satisfactory results.

504 These three reconstructions show that the CaSSIS DEM data is suitable to perform a satisfactory
505 reconstruction that reproduces the expected volume distribution as informed by the morphology.
506 Moreover, the spatial resolution of CaSSIS DEM is sufficient to resolve the ejecta structures observed
507 on the images and that affect the landslide deposit. CaSSIS data can therefore be used to increase the
508 amount of data already available for this type of reconstruction. Furthermore, with acquisitions
509 covering a larger area, ~441 km² (Thomas et al., 2017) compared to ~360 km² for HiRISE (McEwen et
510 al., 2007), CaSSIS is able to image larger landslides, hence filling a gap in the dataset.

511 ## 7. Conclusions

512 Our successful reconstruction of pre-landslide topography with a CaSSIS DEM means that these data
513 can be added to the already available coverage of high-resolution stereo-topographic data with CTX
514 and/or HiRISE. By using three different reconstruction methods from the simplest to the more complex
515 has allowed us to show that CaSSIS data can be used to perform successful and detailed topographic
516 reconstructions. We evaluated this by considering the quantifiable balance between erosion and
517 deposition and more subjectively by considering whether the volume distribution matched what was
518 expected based on the morphology in images alone. In the case of the specific landslide studied in
519 Baetis Chaos, the more complex method, using a tilted plane, produced the best estimates of both
520 volume and mass distribution of the landslide. If only a volume estimate is required, we found that the
521 simplest semi-automatic method produces a satisfactory result and would be suitable to implement
522 for any topographic dataset where large amounts of data are needed for statistical studies. The tilted-
523 plane method is more suited for detailed individual landslide studies, where the landslide is in a
524 complex topographic setting and accurate deposit thickness distributions are required. The CaSSIS
525 ability to acquire a pair of stereo images in a single pass increases the stereographic data coverage of
526 the martian surface. Landslides > 15 km long can currently be studied with MOLA or HRSC data, while
527 landslides < 5 km long can be studied using HiRISE data. CTX data is similar in resolution to CaSSIS, but
528 because of differing surface illumination conditions, acquisition geometry and time interval between
529 images used for stereo, it is not always possible to create a CTX DEM. In addition to providing colour
530 images of the surface, CaSSIS can partially fill the DEM data gap for landslides and other structures
531 between 5 and 15 km in size.

532 ## Acknowledgments

533 SJC, NM and AG are grateful for the support of the Programme National de Planétologie and the French
534 Space Agency (CNES). The authors thank the spacecraft and instrument engineering teams for the
535 successful completion and operation of CaSSIS. CaSSIS is a project of the University of Bern funded
536 through the Swiss Space Office via ESA's PRODEX programme. The instrument hardware development
537 was also supported by the Italian Space Agency (ASI) (ASI-INAF agreement no. I/018/12/0), INAF/
538 Astronomical Observatory of Padova, and the Space Research Center (CBK) in Warsaw. The 3DPD
539 software development was supported by ASI-INAF agreement no. 2020-17-HH.0 and UNIBe. Support
540 from SGF (Budapest), the University of Arizona (LPL), NASA and Manish Patel (UK Space Agency) are
541 also gratefully acknowledged. This study has been supported by the Italian Space Agency (ASI-

INAF agreement no. 2020-17-HH.0). SJC and AN acknowledge the financial support from Région Pays de la Loire, project étoiles montantes METAFLOWS (convention N° 2019-14294).

References

Acton, C.H., 1996. Ancillary data services of NASA's Navigation and Ancillary Information Facility. Planetary and Space Science, Planetary data system 44, 65–70. https://doi.org/10.1016/0032-0633(95)00107-7

Brunetti, M.T., Guzzetti, F., Cardinali, M., Fiorucci, F., Santangelo, M., Mancinelli, P., Komatsu, G., Borselli, L., 2014. Analysis of a new geomorphological inventory of landslides in Valles Marineris, Mars. Earth and Planetary Science Letters 405, 156–168. https://doi.org/10.1016/j.epsl.2014.08.025

Chen, R.-F., Chan, Y.-C., Angelier, J., Hu, J.-C., Huang, C., Chang, K.-J., Shih, T.-Y., 2005. Large earthquake-triggered landslides and mountain belt erosion: The Tsaoling case, Taiwan. Comptes Rendus Geoscience 337, 1164–1172. https://doi.org/10.1016/j.crte.2005.04.017

Chew, L.P., 1989. Constrained delaunay triangulations. Algorithmica 4, 97–108. https://doi.org/10.1007/BF01553881

Coleman, N.M., Baker, V.R., 2009. Surface morphology and origin of outflow channels in the Valles Marineris region, in: Burr, D.M., Carling, P.A., Baker, V.R. (Eds.), Megaflooding on Earth and Mars. Cambridge University Press, Cambridge, pp. 172–193. https://doi.org/10.1017/CBO9780511635632.009

Conoscenti, C., Ciaccio, M., Caraballo-Arias, N.A., Gómez-Gutiérrez, Á., Rotigliano, E., Agnesi, V., 2015. Assessment of susceptibility to earth-flow landslide using logistic regression and multivariate adaptive regression splines: A case of the Belice River basin (western Sicily, Italy). Geomorphology, Geomorphology in the Geocomputing Landscape: GIS, DEMs, Spatial Analysis and statistics 242, 49–64. https://doi.org/10.1016/j.geomorph.2014.09.020

Conway, S.J., Balme, M.R., 2014. Decameter thick remnant glacial ice deposits on Mars. Geophysical Research Letters 41, 5402–5409. https://doi.org/10.1002/2014GL060314

Crosta, G.B., Blasio, F.V.D., Frattini, P., 2018a. Global Scale Analysis of Martian Landslide Mobility and Paleoenvironmental Clues. Journal of Geophysical Research: Planets 123, 872–891. https://doi.org/10.1002/2017JE005398

Crosta, G.B., Frattini, P., Valbuzzi, E., 2013. A New Inventory of Martian Landslides. Presented at the Lunar and Planetary Science Conference, p. 2283.

Crosta, G.B., Frattini, P., Valbuzzi, E., Blasio, F.V.D., 2018b. Introducing a New Inventory of Large Martian Landslides. Earth and Space Science 5, 89–119. https://doi.org/10.1002/2017EA000324

Cruden, D., Varnes, D.J., 1996. Landslide Types and Processes. Special Report - National Research Council, Transportation Research Board 247, 36–57.

de Haas, T., Conway, S.J., Krautblatter, M., 2015. Recent (Late Amazonian) enhanced backweathering rates on Mars: Paracratering evidence from gully alcoves. Journal of Geophysical Research: Planets 120, 2169–2189. https://doi.org/10.1002/2015JE004915

Gross, C., Wendt, L., Dumke, A., Neukum, G., 2009. Further Evidence for Multiple Flooding Events at Juventae Chasma and Maja Valles, Mars 40, 1890.

Gruen, A.W., 1985. Adaptive Least Squares Correlation: A Powerful Image Matching Technique. South African Journal of Photogrammetry, Remote Sensing and Cartography 14, 175–187.

Guimpier, A., Conway, S.J., Mangeney, A., Lucas, A., Mangold, N., Peruzzetto, M., Pajola, M., Lucchetti, A., Munaretto, G., Sæmundsson, T., Johnsson, A., Le Deit, L., Grindrod, P., Davis, J., Thomas, N., Cremonese, G., 2021. Dynamics of recent landslides (<20 My) on Mars: Insights from high-resolution topography on Earth and Mars and numerical modelling. Planetary and Space Science 206, 105303. https://doi.org/10.1016/j.pss.2021.105303

Highland, L., Bobrowsky, P., 2008. The Landslide Handbook – A Guide to Understanding Landslides, Circular 1325. ed, US Geological Survey Circular. US Geological Survey.

Jaboyedoff, M., Chigira, M., Arai, N., Derron, M.-H., Rudaz, B., Tsou, C.-Y., 2019. Testing a failure surface prediction and deposit reconstruction method for a landslide cluster that occurred

during Typhoon Talas (Japan). Earth Surface Dynamics 7, 439–458. https://doi.org/10.5194/esurf-7-439-2019
Legros, F., 2002. The mobility of long-runout landslides. Engineering Geology 63, 301–331. https://doi.org/10.1016/S0013-7952(01)00090-4
Lewis, J.P., 1994. Fast Template Matching. Vis. Interface 95.
Lucas, A., 2010. Dynamique des instabilités gravitaires par modélisation et télédétection: Applications aux exemples martiens (Theses). Institut de physique du globe de paris - IPGP.
Lucas, A., Mangeney, A., 2007. Mobility and topographic effects for large Valles Marineris landslides on Mars. Geophysical Research Letters 34. https://doi.org/10.1029/2007GL029835
Lucas, A., Mangeney, A., Ampuero, J.P., 2014. Frictional velocity-weakening in landslides on Earth and on other planetary bodies. Nature Communications 5. https://doi.org/10.1038/ncomms4417
Lucas, A., Mangeney, A., Mège, D., Bouchut, F., 2011. Influence of the scar geometry on landslide dynamics and deposits: Application to Martian landslides. Journal of Geophysical Research: Planets 116. https://doi.org/10.1029/2011JE003803
Magnarini, G., Mitchell, T.M., Grindrod, P.M., Goren, L., Schmitt, H.H., 2019. Longitudinal ridges imparted by high-speed granular flow mechanisms in martian landslides. Nature Communications 10, 1–7. https://doi.org/10.1038/s41467-019-12734-0
McEwen, A.S., 1989. Mobility of large rock avalanches: Evidence from Valles Marineris, Mars. Geology 17, 1111–1114. https://doi.org/10.1130/0091-7613(1989)017<1111:MOLRAE>2.3.CO;2
McEwen, Eliason, Bergstrom, Bridges, Hansen, C.J., Delamere, Grant, Gulick, Herkenhoff, Keszthelyi, Kirk, Mellon, Squyres, Thomas, Weitz, 2007. Mars Reconnaissance Orbiter's High Resolution Imaging Science Experiment (HiRISE). Journal of Geophysical Research: Planets 112. https://doi.org/10.1029/2005JE002605
Neukum, G., Jaumann, R., HRSC Co-Investigator, Experiment Team, 2004. HRSC: the High Resolution Stereo Camera of Mars Express 1240, 17–35.
Okubo, C.H., 2010. Structural geology of Amazonian-aged layered sedimentary deposits in southwest Candor Chasma, Mars. Icarus 207, 210–225. https://doi.org/10.1016/j.icarus.2009.11.012
Pajola, M., Mergili, M., Cambianica, P., Lucchetti, A., Brunetti, M.T., Guimpier, A., Mastropietro, M., Munaretto, G., Conway, S., Beccarelli, J., Cremonese, G., 2022. Modelling reconstruction and boulder size-frequency distribution of a young (<5 Myr) landslide located in Simud Vallis floor, Mars. Icarus 375, 114850. https://doi.org/10.1016/j.icarus.2021.114850
Pajola, M., Rossato, S., Baratti, E., Mangili, C., Mancarella, F., McBride, K., Coradini, M., 2016. The Simud–Tiu Valles hydrologic system: A multidisciplinary study of a possible site for future Mars on-site exploration. Icarus 268, 355–381. https://doi.org/10.1016/j.icarus.2015.12.049
Quantin, C., Allemand, P., Delacourt, C., 2004. Morphology and geometry of Valles Marineris landslides. Planetary and Space Science 52, 1011–1022. https://doi.org/10.1016/j.pss.2004.07.016
Re, C., Tulyakov, S., Simioni, E., Mudric, T., Cremonese, G., Thomas, N., 2019. PERFORMANCE EVALUATION OF 3DPD, THE PHOTOGRAMMETRIC PIPELINE FOR THE CASSIS STEREO IMAGES. The International Archives of Photogrammetry, Remote Sensing and Spatial Information Sciences XLII-2/W13, 1443–1449. https://doi.org/10.5194/isprs-archives-XLII-2-W13-1443-2019
Rodriguez-Gonzalez, A., Fernandez-Turiel, J.L., Perez-Torrado, F.J., Gimeno, D., Aulinas, M., 2010. Geomorphological reconstruction and morphometric modelling applied to past volcanism. Int J Earth Sci (Geol Rundsch) 99, 645–660. https://doi.org/10.1007/s00531-008-0413-1
Sharp, R.P., 1973. Mars: Fretted and chaotic terrains. Journal of Geophysical Research (1896-1977) 78, 4073–4083. https://doi.org/10.1029/JB078i020p04073
Simioni, E., Re, C., Mudric, T., Cremonese, G., S.Tulyakov, S., Petrella, A., Pommerol, A., Thomas, N., 2021. 3dpd: A Photogrammetric Pipeline For A Push Frame Stereo Cameras. Planetary and Space Science 105165. https://doi.org/10.1016/j.pss.2021.105165
Smith, D.E., Zuber, M.T., Frey, H.V., Garvin, J.B., Head, J.W., Muhleman, D.O., Pettengill, G.H., Phillips, R.J., Solomon, S.C., Zwally, H.J., Banerdt, W.B., Duxbury, T.C., Golombek, M.P., Lemoine, F.G.,

Neumann, G.A., Rowlands, D.D., Aharonson, O., Ford, P.G., Ivanov, A.B., Johnson, C.L., McGovern, P.J., Abshire, J.B., Afzal, R.S., Sun, X., 2001. Mars Orbiter Laser Altimeter: Experiment summary after the first year of global mapping of Mars. Journal of Geophysical Research: Planets 106, 23689–23722. https://doi.org/10.1029/2000JE001364

Stein, A., Meer, F.D. van der, Gorte, B. (Eds.), 2002. Spatial Statistics for Remote Sensing, Remote Sensing and Digital Image Processing. Springer Netherlands. https://doi.org/10.1007/0-306-47647-9

Tanaka, K.L., Skinner, J.A., Dohm, J.M., Irwin, R.P., Kolb, E.J., Fortezzo, C.M., Platz, T., Michael, G.G., Hare, T.M., 2014. Scientific Investigations Map (Scientific Investigations Map).

Thomas, N., Cremonese, G., Ziethe, R., Gerber, M., Brändli, M., Bruno, G., Erismann, M., Gambicorti, L., Gerber, T., Ghose, K., Gruber, M., Gubler, P., Mischler, H., Jost, J., Piazza, D., Pommerol, A., Rieder, M., Roloff, V., Servonet, A., Trottmann, W., Uthaicharoenpong, T., Zimmermann, C., Vernani, D., Johnson, M., Pelò, E., Weigel, T., Viertl, J., De Roux, N., Lochmatter, P., Sutter, G., Casciello, A., Hausner, T., Ficai Veltroni, I., Da Deppo, V., Orleanski, P., Nowosielski, W., Zawistowski, T., Szalai, S., Sodor, B., Tulyakov, S., Troznai, G., Banaskiewicz, M., Bridges, J.C., Byrne, S., Debei, S., El-Maarry, M.R., Hauber, E., Hansen, C.J., Ivanov, A., Keszthelyi, L., Kirk, R., Kuzmin, R., Mangold, N., Marinangeli, L., Markiewicz, W.J., Massironi, M., McEwen, A.S., Okubo, C., Tornabene, L.L., Wajer, P., Wray, J.J., 2017. The Colour and Stereo Surface Imaging System (CaSSIS) for the ExoMars Trace Gas Orbiter. Space Sci Rev 212, 1897–1944. https://doi.org/10.1007/s11214-017-0421-1

Thomas, N., Pommerol, A., Almeida, M., Read, M., Cremonese, G., Simioni, E., Munaretto, G., Weigel, T., 2022. Absolute calibration of the Colour and Stereo Surface Imaging System (CaSSIS). Planetary and Space Science 211, 105394. https://doi.org/10.1016/j.pss.2021.105394

Tsutsui, K., Rokugawa, S., Nakagawa, H., Miyazaki, S., Cheng, C., Shiraishi, T., Yang, S., 2007. Detection and Volume Estimation of Large-Scale Landslides Based on Elevation-Change Analysis Using DEMs Extracted From High-Resolution Satellite Stereo Imagery. IEEE Transactions on Geoscience and Remote Sensing 45, 1681–1696. https://doi.org/10.1109/TGRS.2007.895209

Watson, D., 1999. The natural neighbor series manuals and source codes. Computers & Geosciences 25, 463–466. https://doi.org/10.1016/S0098-3004(98)00150-2